Structures 69 (2024) 107328

Contents lists available at ScienceDirect

Structures

journal homepage: www.elsevier.com/locate/structures

# Nonlinear dynamic study on existing masonry-infilled concrete frames retrofitted with timber panels

Andrea Bartolotti, Francesco Smiroldo, Ivan Giongo *

*Department of Civil, Environmental and Mechanical Engineering, University of Trento, Italy*

ARTICLE INFO

*Keywords:*
Seismic retrofit
Infilled RC frames
Timber retrofit
CLT panels
FEM modelling
Incremental dynamic analysis
Simulated design

ABSTRACT

This study investigates the dynamic performance of a timber-based seismic retrofit for existing reinforced concrete (RC) buildings, named RC-TP. The core of the proposed retrofit intervention is the replacement of the existing masonry infills with structural timber panels that are connected to the concrete elements using metal dowel-type fasteners and a timber subframe. The unreinforced frames were designed according to codes in force in the 60 s and 70 s, considering exclusively gravity loads to simulate a condition common to a large part of the built heritage across Europe. The seismic performance of single-storey single-bay frames before and after the application of the RC-TP retrofit was assessed via nonlinear simulations, for which the incremental dynamic analysis method was adopted. The results of the extensive dynamic study show the effectiveness of the RC-TP retrofit in increasing the seismic acceleration resisted by the frames and their base shear capacity and in promoting a more ductile failure mechanism. Some general considerations helpful in guiding the implementation of the retrofit system were also drawn.

## 1. Introduction

Reinforced concrete (RC) buildings with masonry infills are typical of the building stock of many countries and, in the last years, the seismic response of this kind of structure has been extensively investigated [1–5]. Although current construction codes in seismic-prone areas provide design provisions to ensure a satisfactory level of seismic safety to new buildings (e.g., [6–8]), such safety is not guaranteed for older RC structures built before the advent of modern seismic design principles. Consequently, existing structures often have poor seismic detailing due to superseded design/construction practices that can lead to extensive damage and the activation of brittle failures under earthquake loading [9–12]. When approaching the seismic assessment of RC frame structures, it is now widely acknowledged that the effect of the infills on the overall seismic response must be accounted for, an aspect often neglected in past designs. An increasing number of studies in the literature confirm that in the case of seismic events the *masonry infill-RC frame* interaction can involve additional shear actions on the structural elements and unexpected collapse mechanisms [13,14]. Specifically, soft story mechanisms can be activated by a concentration of deformations in a single storey due to irregular vertical distributions of the infills or by torsional effects due to irregular horizontal distributions [15], [16]. Additionally, soft-story mechanisms can activate also in the case of RC frames with uniformly distributed infills when the early collapse of the infills at lower stories generates vertical irregularities [17]. In addition, failure of the RC elements caused by local frame-infill interaction is favoured by strong infills in weak frames [18], [19] due to the diagonal compression strut developing in the masonry. The horizontal forces are transferred by the strut to the opposite ends of the contiguous columns generating a concentration of stress that can cause them to fail in shear [20], [21]. The so-called “short column” effect can also lead to similar consequences [22].

Different approaches can be adopted to reduce the seismic vulnerability of existing infilled RC frames depending on the specific goal. Some techniques aim at strengthening the infill to avoid their collapse [23–25], other at limiting the detrimental effects of the in-plane infill-to-frame interaction [26], or increasing the lateral capacity of the structural system [27], [28]. The recent flourishing of integrated retrofit strategies that target not just the structural performance but also the energy efficiency of the existing buildings, has brought further attention to the retrofit of masonry infill walls. Several examples of such integrated retrofits can be found in [29,30].

The possibility of using timber panels for retrofitting RC buildings recently caught the attention of the scientific community and timber-

* Corresponding author.
*E-mail address:* ivan.giongo@unitn.it (I. Giongo).

https://doi.org/10.1016/j.istruc.2024.107328
Received 4 January 2024; Received in revised form 30 August 2024; Accepted 17 September 2024

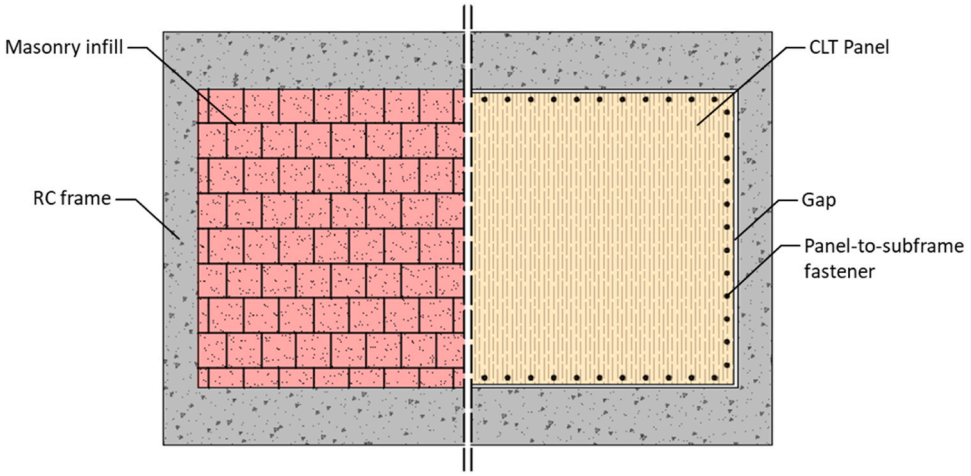


**Fig. 1.** Generic infilled-frame before (on the left) and after (on the right) the application of the retrofit solution.

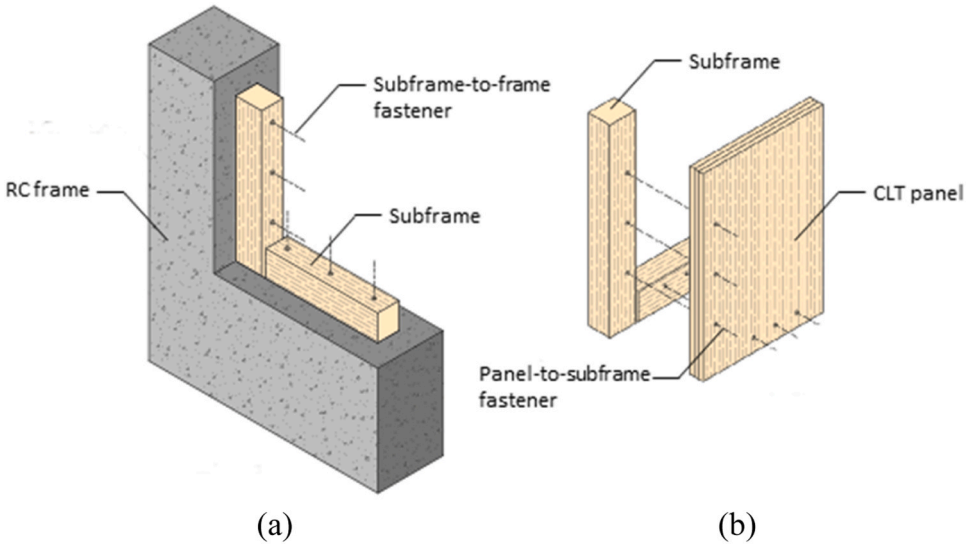


**Fig. 2.** Connection system of the retrofit solution: a) subframe-to-frame connection, b) panel-to-subframe connection.

based techniques have been proposed by a few authors [31]. Sustersic & Dujic [32] have proposed connecting cross-laminated timber (CLT) panels to the outer surface of masonry infilled frames using special steel plates and brackets. They have shown via shake table testing that a masonry infilled-frame damaged by ground motions up to 0.75 g withstood the same 0.75 g earthquake twice without further damage after being retrofitted with the abovementioned technique. Margani et al. [33] have analysed the energy performance of a retrofit concept similar to that in [32], with the *CLT-RC frame* connection made using special steel brackets incorporating friction dampers effective after a connection deformation settlement of approximately 20 mm [34]. A numerical comparison of alternative three-dimensional connectors (including that proposed by [32]) can be found in Mehdipour et al. [35]. Stazi et al. [36], have studied the possibility of using CLT panels as infills, with the RC frame confining the timber panels thanks to fully effective CLT-to-concrete contact. Suga et al. [37], have investigated using relatively short laminated-veneer-lumber (LVL) panels that are glued together and to the RC frame using epoxy resin. The retrofit technique studied herein, introduced by Smiroldo et al. [38–42] and named RC-TP, aims to enhance the seismic response of infilled RC frames through the replacement of the infill walls with cross-laminated timber (CLT) structural panels screwed to a timber subframe fixed inside the frames of the RC structure using dowel-type fasteners. A clearance gap between the faces of the RC columns/beams and the edges of the CLT facilitates the panel installation and prevents direct panel-to-frame contact. Initial numeric studies based on static analyses [38–41] and quasi-static testing up to failure of full-scale specimens [42] showed promising results, with the retrofitted frames having a notably improved response compared to the original masonry infilled configurations. In particular, higher strength, displacement capacity, and a generally more ductile behaviour were observed.

The present study aims to evaluate the effectiveness of the RC-TP retrofit solution through a nonlinear approach, with a novel emphasis on dynamic response. Single record incremental dynamic analyses (IDAs) were conducted on single-storey, single-bay RC frames to represent both infilled and retrofitted configurations. This approach was chosen to investigate the retrofit's performance under dynamic loading conditions at a component level. To fully capture the variability in seismic response of entire buildings, multiple records are typically required. However, given the primarily exploratory nature of the study, which focuses on a single degree of freedom structural component, only one single spectrum-compatible record was selected. Future research should extend this analysis to a building scale, incorporating a broader range of ground motions to provide a more comprehensive evaluation of seismic action and structural response. Within such research boundaries, a design strategy was developed to optimize the retrofit intervention by

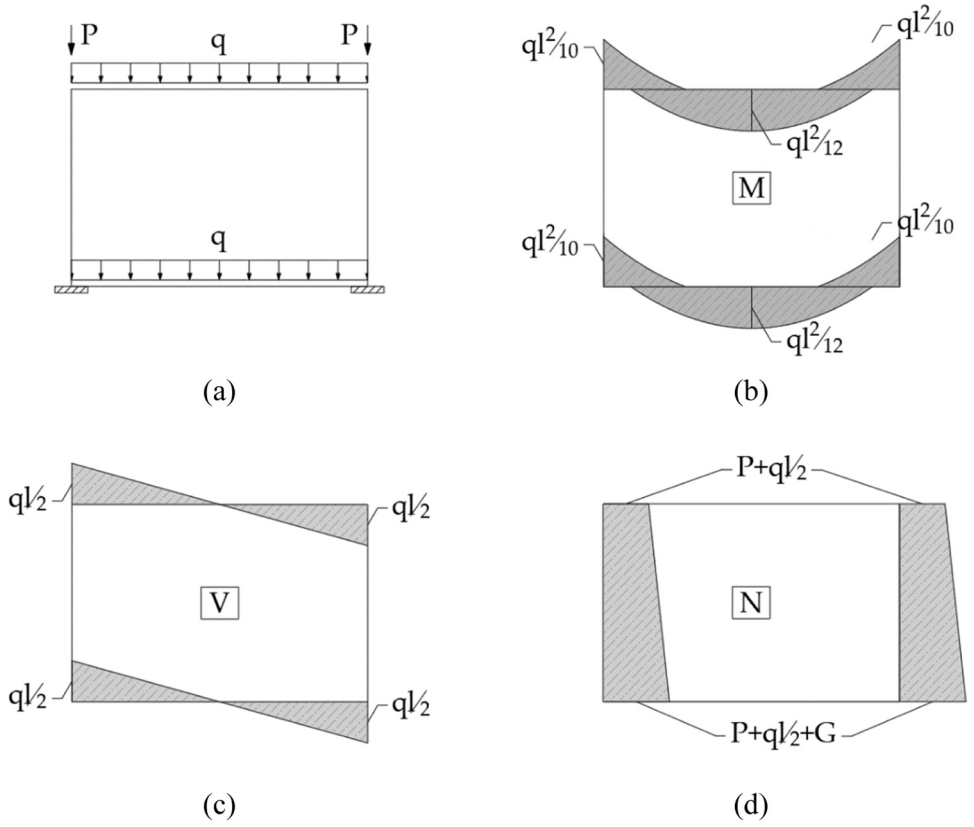


**Fig. 3.** Distribution of external and internal actions adopted in the design simulation – *P*, column concentrated load; *q*, beam distributed load; *l*, beam length; *G*, column weight: a) external actions; b) bending moment diagram; c) shear force diagram; d) axial force diagram.

performing a parametric study addressing one of the most critical retrofit parameters: the connections.

## 2. Retrofit technique

The retrofit technique investigated in the present paper has been described in detail in [38–42]. The intervention involves replacing the masonry infills with CLT structural panels (Fig. 1). The load transfer between the panel and the RC frame is ensured by a connection system comprising a timber subframe (Fig. 2a), subframe-to-frame fasteners (Fig. 2a) and panel-to-subframe fasteners (Fig. 1 and Fig. 2b). To prevent the transfer of additional shear forces to the RC frame via direct contact with the CLT panel, a gap is maintained between the internal surfaces of the RC frame and the panel edges (Fig. 1). This gap, with a width of approximately 1.5 to 3 cm, is designed to accommodate the deformation of the fasteners. By doing so, it ensures that, until complete failure of the connection, stress between the panel and the RC frame is transferred solely by the fasteners, thereby avoiding the development of a compressed strut within the CLT panel.

Both the subframe-to-frame connection (RC-Conn) and the panel-to-subframe connection (T-Conn) consist of metal dowel-type fasteners. The RC-Conn can be made with dry concrete-screws or with resin-bonded steel anchors, depending on the characteristics of the concrete material and on the resistance demand. The T-Conn is obtained by using partially threaded timber screws with washers inserted perpendicularly to the panel surface.

Furthermore, the RC-Conn is designed to be significantly stiffer than the T-Conn. Therefore, in the modelling phase, the RC-Conn was assumed to be rigid. On the other hand, the T-Conn, which governs the force transfer between the concrete frame and the timber panel, was calibrated to exceed the elastic range before the collapse of the frame elements. The post-elastic resources of the timber screw connections add to the system energy dissipation.

In addition, the strong direction of the CLT panel is oriented vertically (i.e., the external layers of the panel have the boards running vertically). In fact, in the event of severe damage to the structural elements, the CLT panels can provide additional vertical load support by redistributing the loads across the damaged areas, acting as secondary load paths. The contact forces developing at the gap closure between the panel and the RC beams allows for the vertical load transmission as reported also in [41] and [42]. However, further studies are needed to investigate the progressive collapse mechanisms that RC-TP retrofitted buildings may experience due to strong ground motions. These studies would provide valuable insights for designing RC-TP retrofits that can ensure the stability of the structure, even in case of RC member failures.

## 3. Definition of the frame characteristics

In the present study, four different single-storey single-bay infilled RC frames were considered. The frames are intended to be representative of existing RC structures designed for gravity loads only. The period of maximum production of RC buildings in Italy was between 1960 and 1980 [43]. During those two decades, design codes changed. In 1972, the design code in force since 1939 [44] and the associated explanatory document [45] were replaced by [46]. Therefore, the existing RC frames considered in the analyses were divided into two sets composed of two frames each. The first set of frames, referred to as “60s frames”, follows the provisions of the older design codes [44], [45]. The frames in the second set were instead designed following the provisions of [46] and will be referred to as “70s frames”.

Once the material properties, cross-section geometry, aspect ratios, and vertical loads were defined, a design simulation was performed to determine the details of the frame reinforcement. Several aspects of common design practice, such as the use of bent longitudinal bars at the

**Table 1**
Design strengths relative to the considered periods: $\sigma_{cc,R}$, concrete allowable compressive stress for axial forces; $\sigma_{cf,R}$, concrete allowable compressive stress for bending; $\tau_{c,0}$, maximum concrete shear stress in the absence of shear reinforcement; $\tau_{c,max}$, concrete allowable shear stress when shear reinforcement is present; $\sigma_{s,R}$, steel rebar allowable tensile stress.

| Period | Concrete | | | | Steel | |
|---|---|---|---|---|---|---|
| | $\sigma_{cc,R}$ [kg/cm$^2$] | $\sigma_{cf,R}$ [kg/cm$^2$] | $\tau_{c,0}$ [kg/cm$^2$] | $\tau_{c,max}$ [kg/cm$^2$] | Type | $\sigma_{s,R}$ [kg/cm$^2$] |
| 60s | 45,00 | 55,00 | 6,00 | 16,00 | Aq50 | 1600 |
| 70s | 59,90 | 85,00 | 5,33 | 15,33 | FeB32 | 1600 |

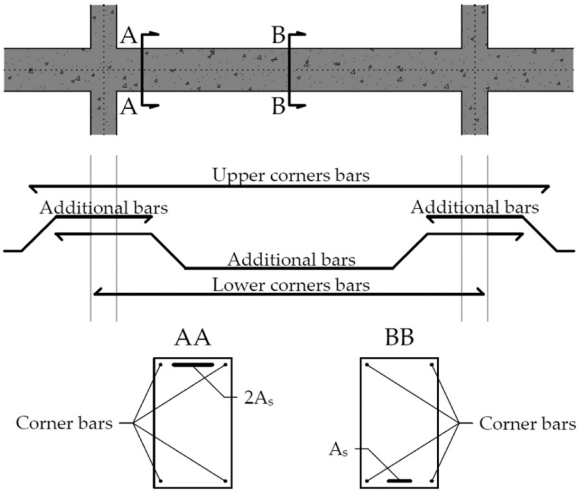


**Fig. 4.** Layout of longitudinal reinforcement typical of RC beams constructed between 1960 and 1980 ($A_s$ = area of the longitudinal reinforcement bars supplementing the corner bars to meet the design requirements).

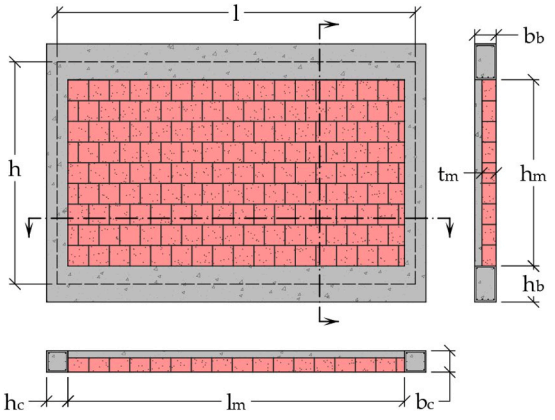


**Fig. 5.** Geometrical characteristics of the considered frames.

end of the beams or the assumed distribution of internal forces (Fig. 3) were deduced from old design manuals [47,48].

Consistently with the reference construction codes for both the 60s and the 70s frames, the design was carried out according to the method known as "allowable stress". The design strength values adopted in the present study were derived from the most typical materials used during the considered periods [44,46] and are reported in Table 1.

A particularly interesting provision by the standards previously mentioned concerns the detailing of transverse reinforcement in columns. The construction code used for designing 60s frames prescribes a maximum spacing $s_{max}$ for stirrups equal to:

**Table 2**
Mechanical and geometrical properties of the analysed frames.

| Material properties | | | Geometry | |
|---|---|---|---|---|
| **Concrete** | 60 s | 70 s | **Frame** | |
| Compressive strength, $f_c$ (MPa) | 17,00 | 24,00 | Beam span, l (cm) | 500 |
| Modulus of elasticity, $E_c$ (GPa) | 26,30 | 29,50 | Storey height, h (cm) | 310 |
| **Rebar** | 60 s | 70 s | **Beam section** | |
| Yielding stress, $f_y$ (MPa) | 380 | 430 | Beam height, $h_b$ (cm) | 50 |
| | | | Beam width, $b_b$ (cm) | 30 |
| **Masonry infill (hollow clay bricks)** | | | | |
| Compressive strength, $f_m$ (MPa) | 6,50 | | **Column section** | |
| Modulus of elasticity, $E_m$ (GPa) | 4,55 | | Column height, $h_c$ (cm) | 30 |
| Basic shear strength, $f_{v0}$ (MPa) | 0,13 | | Column width, $b_c$ (cm) | 30 |
| Diagonal shear strength, $f_{v0m}$ (MPa) | 0195 | | | |
| | | | **Infill** | |
| **Loads** | | | Infill thickness, $t_m$ (cm) | 20 |
| | | | Infill height, $h_m$ (cm) | 260 |
| **Column load** | Low | High | Infill length, $l_m$ (cm) | 470 |
| Top column axial force, P (kN) | 100 | 340 | | |
| **Beam load** | | | | |
| Beam distributed load, q (kN/m) | 15 | | | |

$$s_{max} = \min\left(0.5\min(b,h),\quad 10\varnothing_{long}\right)$$

Taking into account the usual longitudinal bar diameters (ranging between 12 and 16 mm [49]) and the typical minimum cross-section geometry of the columns (300 ×300 mm [25]), the "$s_{max}$" limitation for the 60s frames is more severe than that used for designing 70s frames, which instead is:

$$s_{max} = \min\left(25\text{ cm},\quad 15\varnothing_{long}\right)$$

For this reason, the columns of 60s frames may exhibit higher shear strength than the columns of 70s frames.

Regarding transverse reinforcement of the beams, the 60s design code does not specify a maximum spacing for stirrups. However, the code states that if the shear stress exceeds $\tau_{c,0}$, the entire shear force must be absorbed by the steel reinforcement made of sole stirrups or stirrups and bent longitudinal bars. Additionally, at least 50 % of the shear force must be attributed to stirrups. A similar requirement is also present in the 70s standard, where the minimum percentage of shear force to be attributed to the stirrups is 40 % and where the minimum transverse reinforcement is specified and amounts to three stirrups per meter length of beam.

For the beam design, a typical layout of the longitudinal reinforcement was adopted [47,48], and it is shown in Fig. 4.

To investigate the influence of the column axial load, the two mentioned sets were divided into two subsets that differ in the magnitude of the compression force at the top of the columns. For brevity, these subsets will be referred to as "high column load" (HCL) and "low column load" (LCL). Vertical forces are consistent with the loading of columns located on the ground floor of a two-storey and of a four-storey building, respectively. The distributed gravity load assigned to the beam (15 kN/m) is consistent with the load from medium-weight infills with openings and medium-weight floors (≈2.5 m tributary length). The geometrical properties, load assignments, and material properties

**Table 3**
Steel reinforcement of the frames.

| **Beam details** | | | | | |
|---|---|---|---|---|---|
| | **At support** | | **At midspan** | | **Stirrups** |
| | Extrados | Intrados | Extrados | Intrados | |
| 60 s | 6Ø16 | 2Ø16 | 2Ø16 | 4Ø16 | Ø6/17 |
| 70 s | 4Ø14 + 2Ø10 | 2Ø14 | 2Ø10 | 4Ø14 | Ø6/30 |
| **Column details** | | | | | |
| | **Load level** | | **Stirrups** | | |
| | Low | High | | | |
| 60 s | 4Ø12 | 8Ø12 | Ø6/20 | | |
| 70 s | 4Ø12 | 8Ø12 | Ø6/18 | | |

*X*ØY = X number of bars of diameter Y mm
ØY/Z = Stirrups of Y mm diameter spaced at Z cm

**Table 4**
Retrofit configurations considered in the analysis of each frame subset.

| **Name** | **Fastener spacing along beams** | **Fastener spacing along columns** |
|---|---|---|
| MI | - | - |
| R 10 −20 | 10 cm | 20 cm |
| R 10 −55 | 10 cm | 55 cm |
| R10-NO | 10 cm | No fasteners |
| R 20 −20 | 20 cm | 20 cm |
| R 20 −55 | 20 cm | 55 cm |
| R 20-NO | 20 cm | No fasteners |

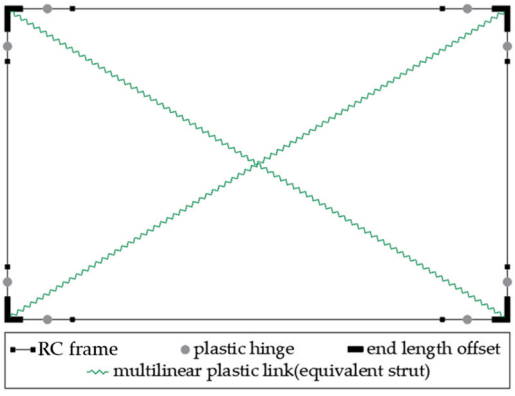


**Fig. 6.** Numerical model of the masonry infilled-frame.

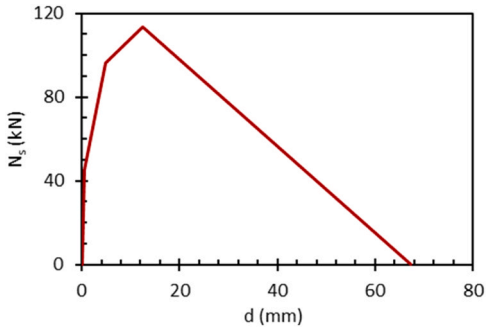


**Fig. 7.** Constitutive law for the equivalent strut (masonry infill) in compression: Ns, axial load; d, axial displacement.

adopted in the frame models are reported in Fig. 5, Table 2 and Table 3. The mechanical properties of the materials correspond to typical values for existing RC buildings dated to the periods considered by this study

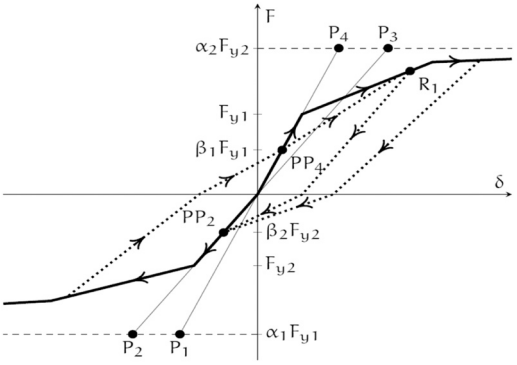


**Fig. 8.** Hysteretic Pivot model for a generic tension-compression rule [55,57].

**Table 5**
Pivot model parameters adopted in the analyses.

| | $\alpha_1$ | $\alpha_2$ | $\beta_1$ | $\beta_2$ |
|---|---|---|---|---|
| Equivalent strut | 0,00 | 0,25 | 0,00 | 0,00 |
| Fasteners | 100,00 | 100,00 | 0,40 | 0,40 |

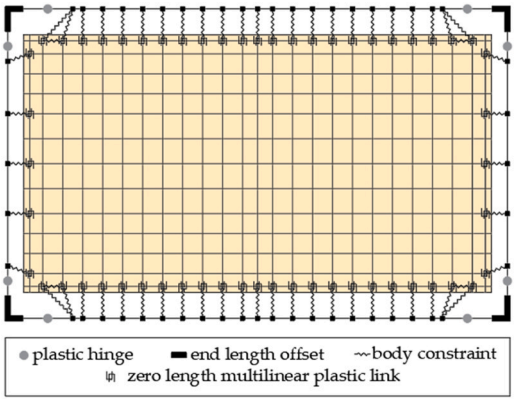


**Fig. 9.** Retrofitted frame numerical model.

[49–51].

Each subset comprises frames in the “as-built” configuration and several alternative retrofit configurations, which involve different spacings of the panel-to-subframe fasteners along the columns and beams. In the following, the frames representing the as-built configuration are identified by the acronym "MI" (i.e., masonry infilled).

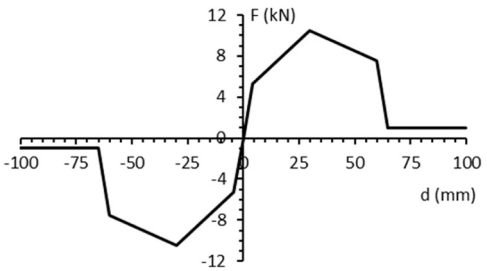


**Fig. 10.** Backbone curve of the panel-to-subframe connection: F, shear force acting on the connection; d, connection slip.

Instead, the retrofitted frames are identified using the letter "R" followed by a pair of numbers that indicate the fastener spacing (in centimetres) along beams and columns, respectively. In the case of no fasteners, "NO" replaces the spacing number on the label. The configurations analysed for every subset are summarized in Table 4. The seven configurations per subset resulted in a total of 28 different models.

## 4. Numerical modelling

The modelling strategy adopted in the present study was defined based on the one presented in [40]. Some changes were introduced to make it suitable for nonlinear dynamic analysis (e.g., by adding hysteretic material response), to reduce computational burden, and facilitate the model creation process. Consistently with the previous stages of the research reported in [38–42], 2-dimensional in-plane analyses were performed using the software SAP2000 [53].

The RC structure is made up of straight frames that represent the beam and column members. *Fibre hinges* are introduced to simulate the nonlinear material behaviour via a concentrated plasticity approach. The higher stiffness of the joints is accounted for by assigning rigid *end-offsets* to the beams and columns. Because of that, the joint strength verification was carried out *a posteriori*.

Due to the adoption of fibre hinges, the nonlinear bending response of the RC components is directly derived from the constitutive law of the materials. Specifically, the Mander model [54] was adopted for concrete, neglecting confinement effects. Steel reinforcement, instead, is characterized by a uniaxial elastic-perfectly plastic law. The hysteretic behaviour of materials was also considered: the kinematic hysteresis model was adopted for steel reinforcement, while the built-in "concrete" hysteresis model [53] was used to describe the cyclic behaviour of concrete.

With reference to the as-built configurations (MI), the masonry infills are simulated using the concentric equivalent strut macro-model visible in Fig. 6. The modelling approach proposed by [55] was adopted for the characterization of the equivalent struts and their backbone curves

**Table 6**
Main geometrical properties of the reference frames for the numerical model experimental validation.

| **Frame:** | | **Infill:** | |
|---|---|---|---|
| Beam span (cm): | 460 | Solid clay bricks wythe: | |
| Storey height (cm): | 275 | Thickness (cm): | 12 |
| Beam height (cm): | 40 | Height (cm): | 235 |
| Beam width (cm): | 30 | Length (cm): | 430 |
| Column height (cm): | 30 | | |
| Column with (cm): | 30 | Hollow clay bricks wythe: | |
| Beam reinforcement (support): | 6Ø14 + 2Ø14 | Thickness (cm): | 8 |
| Column reinforcement: | 4Ø14 | Height (cm): | 235 |
| | | Length (cm): | 430 |
| **Retrofit configuration:** | | **Load:** | |
| Configuration: | R−10-NO | | |
| T-Conn fasteners diameter (mm): | 10 | Top column axial force (kN): | 220 |
| Panel thickness (cm): | 10 | Beam distributed load (kN/m): | 16 |

**Table 7**
Mechanical properties of the reference frames derived from [62].

| **Concrete** | | **Strong/weak masonry wythe** | |
|---|---|---|---|
| Compressive strength (MPa): | 10.0 | Compressive strength (MPa): | 10.4/1.6 |
| Modulus of elasticity (GPa): | 22000 | Modulus of elasricity (MPa): | 10400/1600 |
| | | Diagonal shear strength (MPa): | 0.25/0.15* |
| **Steel bars** | | **Steel fasteners** | |
| Yielding strength (MPa): | 532 | | |
| Modulus of elasticity (MPa): | 206000 | Maximum shear strength (kN): | 14.4 |
| | | Ultimate displacement (mm): | 45 |

* In the absence of experimental data, the value was assumed as recommended by [52].

a) b)

**Fig. 11.** RC frames tested in [42] and referred to for the numerical model validation: a) infilled frame b) retrofitted frame.

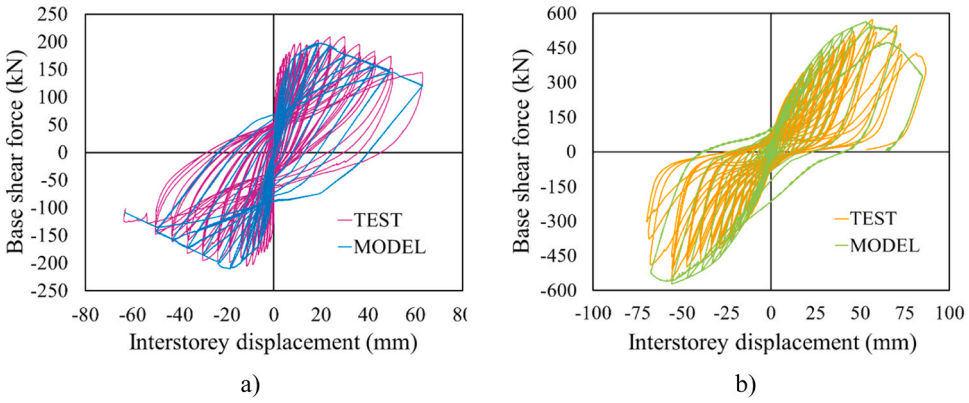


**Fig. 12.** Validation of the numerical models based on the results of experimental quasi-static cyclic tests: a) infilled frame; b) retrofitted frame.

**Table 8**
Natural accelerogram selected from the PEER database.

| Earthquake Name | Station Name | Year | Magnitude | 5-95 % Duration (sec) |
|---|---|---|---|---|
| Imperial Valley−02 | EI Centro Arry #9 | 1940 | 6,95 | 24,2 |

(Fig. 7). The hysteretic behaviour of the infill is described using the Pivot hysteresis model [56] according to [57]. To define the Pivot model (Fig. 8), a strength envelope must first be selected by assigning yield force values in tension and compression ($F_{y1}$ and $F_{y2}$), initial stiffness, and peak strength. The hysteresis rules are then governed by the parameters $\alpha_1$, $\alpha_2$, $\beta_1$ and $\beta_2$ (Fig. 8). As shown in Fig. 8, the primary points (P1 and P2, P3 and P4) and the pinching points (PP2 and PP4) lie on the lines containing the elastic branches of the strength envelope where the y-axis intercepts $\alpha_2 F_{y2}$ and $\alpha_1 F_{y1}$, and $\beta_1 F_{y1}$ and $\beta_2 F_{y2}$, respectively. Because the equivalent strut acts only in compression and the experimental evidence available in the literature has shown that the infills do not gain stiffness when the load is reversed until the total plastic deformation is recovered [57], the parameters $\alpha_1$, $\beta_1$ and $\beta_2$ are set as null. Therefore, the Pivot model adopted here to describe the hysteretic behaviour of the infilled frame requires only the definition of the $\alpha_2$ parameter. The value assumed for the $\alpha_2$ parameter is reported in Table 5 and was calibrated by [57] based on experimental results obtained from cyclic testing of a clay masonry-infilled RC frame.

To take into account the local interaction between the frame and the infill, provisions by FEMA [58] were considered, as suggested by [59]. Therefore, the shear forces acting on the beam and column elements were estimated by decomposing the axial force acting on the equivalent strut in the vertical and horizontal directions, respectively.

Regarding the retrofitted frame modelling approach (Fig. 9), the timber panel was reproduced by using orthotropic shell elements. As observed in [38], the stress state in the CLT panel during lateral loading was expected not to exceed the elastic strength of the material. Therefore, a linear elastic behaviour was attributed to the shell elements and stress compatibility with the material strength was checked a posteriori.

The panel-to-subframe connection was modelled by means of multilinear plastic links whose properties were derived from [38] and are reported in Fig. 10. A Pivot hysteretic model was also adopted to capture pinching phenomena and characterize the connection behaviour under unloading and reloading conditions (Fig. 8). Such hysteretic model is often used in the literature to simulate timber-to-timber connections [60,61]. The parameters α1, α2, β1, and β2 adopted herein are reported in Table 5. Differently, the subframe-to-frame connection was assumed to be rigid and a "body constraint" between the subframe and the frame was set.

## 5. Model validation on experimental evidence

The modelling approach was validated on the results of an experimental campaign conducted at the Department of Civil Environmental

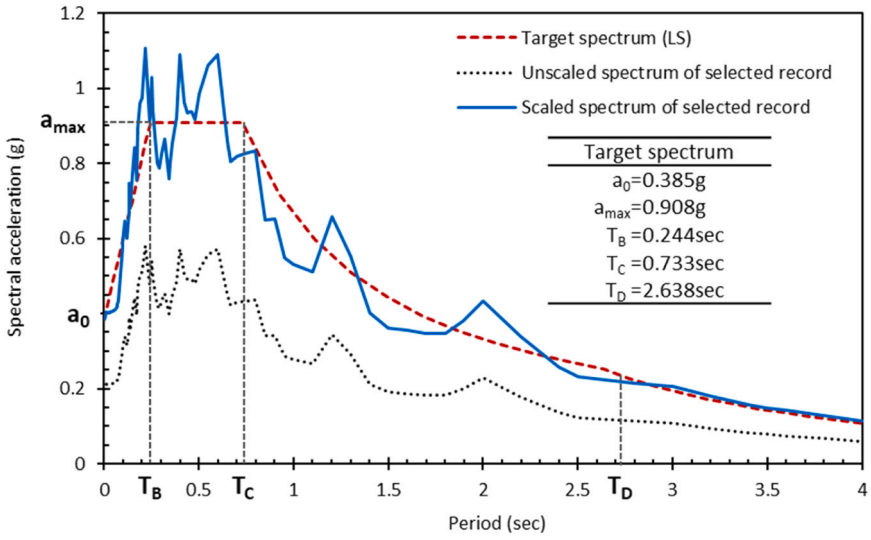


**Fig. 13.** Comparison between the life safety (LS) target spectrum, the unscaled and the scaled spectrum of the selected record.

**Table 9**
Natural period and associated spectral acceleration of the analysed frames.

| Reference period | Column load | Configuration | Natural period (sec) | Spectral acceleration (g) |
|---|---|---|---|---|
| 70s | HCL | MI | 0,16 | 0,81 |
| | | R 10 −20 | 0,32 | 0,86 |
| | | R 10 −55 | 0,33 | 0,81 |
| | | R10-NO | 0,34 | 0,78 |
| | | R 20 −20 | 0,34 | 0,78 |
| | | R 20 −55 | 0,36 | 0,84 |
| | | R 20-NO | 0,38 | 0,91 |
| | LCL | MI | 0,10 | 0,60 |
| | | R 10 −20 | 0,20 | 0,97 |
| | | R 10 −55 | 0,21 | 1,01 |
| | | R10-NO | 0,21 | 1,07 |
| | | R 20 −20 | 0,21 | 1,07 |
| | | R 20 −55 | 0,22 | 1,08 |
| | | R 20-NO | 0,23 | 0,96 |
| 60s | HCL | MI | 0,17 | 0,80 |
| | | R 10 −20 | 0,33 | 0,81 |
| | | R 10 −55 | 0,34 | 0,77 |
| | | R10-NO | 0,36 | 0,85 |
| | | R 20 −20 | 0,36 | 0,84 |
| | | R 20 −55 | 0,37 | 0,90 |
| | | R 20-NO | 0,40 | 1,05 |
| | LCL | MI | 0,10 | 0,61 |
| | | R 10 −20 | 0,21 | 1,01 |
| | | R 10 −55 | 0,21 | 1,07 |
| | | R10-NO | 0,22 | 1,07 |
| | | R 20 −20 | 0,22 | 1,08 |
| | | R 20 −55 | 0,23 | 0,98 |
| | | R 20-NO | 0,25 | 0,99 |

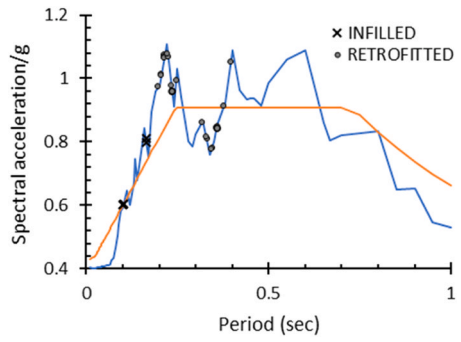


**Fig. 14.** Spectral acceleration at the first mode for the analysed frames.

and Mechanical Engineering of the University of Trento (Italy) [42], in the framework of a collaboration between the University of Trento and the Joint Research Centre in Ispra (Italy). A set of four RC frames, including both as-built masonry-infilled frames and frames retrofitted with RC-TP, was tested under pseudo-static cyclic loading up to collapse. A double-wythe masonry infilled frame (Fig. 11-a) and a frame with the CLT retrofit (Fig. 11-b) were taken as references for the validation of the numerical models. The main geometric properties of the reference frames are reported in Table 6.

The mechanical properties of the concrete, steel rebar, masonry wythes and steel fasteners assigned to the numerical models for the experimental validation were derived from [62] and are summarized in Table 7.

The results of the experimental validation are reported in Fig. 12. Regarding the infilled frame (Fig. 12-a), the numerical simulation adequately matched the experimental response, even though with a slight underestimation of the initial stiffness. The model's prediction of the base shear capacity of the experimental test falls within the 5 % error range. Strength and stiffness degradation was mainly due to damage in the masonry infill in both numerical model and experimental test. As concerns the retrofitted frame, it appears from Fig. 12-b that both the initial stiffness and the base shear capacity were accurately predicted by the numerical model. In the numeric simulation, a combination of frame members' strength degradation and fasteners' failure was responsible for the retrofitted frame collapse, as it has also been observed experimentally.

## 6. Single record IDAs

The seismic performance of the frames was investigated through single-record incremental dynamic analyses [63]. The procedure consists of iterating nonlinear dynamic analyses in which the record is upscaled at every step to increase the seismic intensity. The record used for the analyses (Table 8) was selected from the PEER West2 Database [64], adopting a target design spectrum defined according to the Italian code [65] relative to areas with high seismic hazards.

The target spectrum, the unscaled spectrum and the scaled spectrum of the selected record are reported in Fig. 13.

The peak ground acceleration (PGA) was selected as the intensity measure IM for the present study. The incremental process was performed through a stepping algorithm, where the IM was increased by constant increments from zero to the collapse of the structure.

Table 9 reports the natural periods and the associated accelerations obtained from the scaled spectrum. It can be seen that the natural periods of the retrofitted frames are approximately twice as long as the periods of the infilled frames. Because differences in spectral accelerations can bias the analysis results, it is worth noting that the infilled frames' accelerations are, on average, lower than those of retrofitted frames (Table 9 and Fig. 14). This resulted in a conservative assessment of the effectiveness of the intervention.

During the analyses, the performance of the frame was assessed according to the provisions of the Italian code [65]. Specifically, shear strength, ductility and deformation capacity (evaluated with reference to the rotation of the chords of the members), and joint strength were checked at every step of the analysis. As recommended by [52], RC shear strength degradation under cyclic loading was also taken into account. This phenomenon, which involves a reduction in shear capacity due to the widening of flexural-shear cracks [66], has been widely investigated by [67], who has proposed the formulation currently implemented in Eurocode 8 [6].

## 7. Analysis of results

Given that previous studies [39] have shown that, in the case of especially vulnerable beam-column joints, additional interventions (e.g., by using fiber reinforced polymers) must be adopted to ensure the joint overstrength required by a capacity design approach, the response of the joints was evaluated separately. In the following, the condition of incipient collapse is therefore identified with the failure of a column or a beam element.

The results of the analyses showed that the retrofit intervention can generate a marked improvement in the overall seismic capacity with respect to the masonry-infilled configuration. By considering the retrofit solution that reached the maximum PGA for each frame type (Fig. 15 and Table 10), it is possible to observe: a) an increase in PGA at collapse ($\Delta PGA_u$) ranging from 64 % to 217 %; b) an increase in maximum lateral capacity ($\Delta H_{max}$) ranging from 82 % to 240 %. These improvements are mainly due to the activation of a beam-to-beam load transfer mechanism that reduced the shear force acting on the columns in all analysis runs (Fig. 16). In fact, part of the horizontal force is transferred from the upper beam to the lower one through the timber panel, reducing the involvement of the columns in the shear load transfer mechanism. Expectedly, the beam-to-beam load transfer appears more efficient when the spacing between the fasteners along the beams is

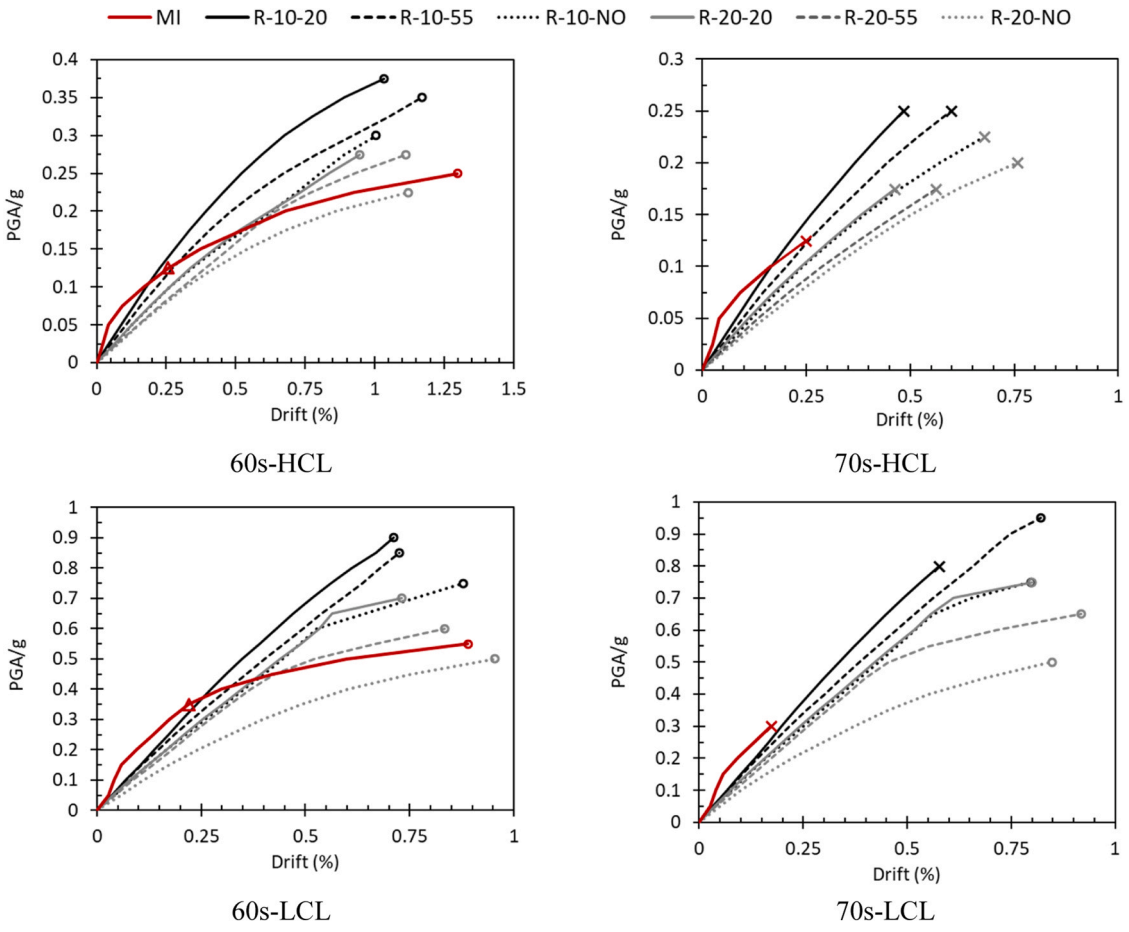


**Fig. 15.** Comparison between as-built and retrofitted configurations – Single record IDA curves (PGA/g – Drift): ○ marker, shear collapse of columns due to cyclic effects; × marker, shear collapse of columns; △ marker, infill collapse.

reduced. The data reported in Table 10 show that the increase in the base shear capacity ($\Delta H_{max}$) due to the retrofit is on average 68 % for frames with fasteners spaced at 20 cm along the beams, while it is 124 % for frames with fasteners spaced at 10 cm. In addition, for a given PGA, the average reduction in column shear demand (Fig. 16) moved from 33 % (20 cm spacing) to 42 % (10 cm spacing). Lastly, from Fig. 15 it is possible to observe that, for the same PGA, the reduction in the spacing of the fasteners along the beams resulted in a reduction of the drift demand for the retrofitted frames.

As visible in Fig. 17, for the same PGA, an increased beam shear demand was found on the retrofitted frames compared to the masonry infilled ones. However, even though older buildings were designed for gravity loads only without considering any appreciable shear action on columns, the transverse reinforcement of the beams was explicitly designed assuming an appropriate safety level for the expected vertical loads. Consequently, these types of buildings usually are much more vulnerable to shear forces applied to the columns rather than to the beams. Therefore, to maximise the benefits of the intervention, it is possible to exploit the shear resistance reserve of the beams. In Fig. 17 it is also possible to observe that the fastener spacing along the columns affects the shear demand on the beams. Moving from configurations with no fasteners on columns to configurations with a 20 cm fastener spacing, an average drop of 20 % in the beams shear demand was found for any given PGA. This response suggests that, in the case of beams with poor shear resistance, configurations with more fasteners on the columns may be more efficient. In any case, in applying the proposed intervention, the increase in the beam shear demand must be accounted for with care.

It is worth noting that, in terms of $\Delta PGA_u$, the 60s retrofitted frames showed an overall minor (yet still significant) improvement in the seismic response compared to the 70s ones. Such a result is to be attributed to the better seismic performance of the 60s frames in the as-built infilled configuration rather than to a lower effectiveness of the retrofit solution. As previously mentioned, due to the building codes in force at the time, the 60s frames are characterized by a higher column shear strength that makes them less vulnerable to the local shear action transferred by the infill. Consequently, for the masonry infilled configurations, the analyses showed greater displacement capacities in the case of 60s frames (e.g., see for example 60s-HCL – 70s-HCL and 60s-LCL – 70s-LCL in Fig. 15). The higher column shear strength of 60s frames involved also the development of ductile failure mechanisms with plastic hinge formation, followed by the cyclic shear strength degradation of the columns. However, it must be noticed that failure of the masonry infill (marked with a red triangle in Fig. 15) occurred for displacement values significantly smaller than those associated to the column shear failure. Developing a ductile response in the infilled configurations requires, therefore, the acceptance of the collapse of the infill, itself a life safety hazard.

In the case of both LCL and HCL, the retrofit interventions generated marked improvements in the seismic response. However, increasing the vertical loads produced opposite results in 60s and 70s frames because of the different characteristics of the column cross-sections. With higher vertical loads, the column yielding and maximum moment increase, causing an increase in the maximum shear. In the case of HCL 70s frames, characterised by a poor shear strength, the increase in shear due to the higher vertical loads (e.g., see R10–55 in Fig. 16) caused the column shear failure, resulting in smaller $\Delta PGA_u$, $\Delta H_{max}$ and $\Delta d_{max}$ (Table 10) compared to the LCL 70s frames. In contrast, in the 60s

**Table 10**
Analysis results: symbol ↑,best performing configuration for each subset; S, shear collapse; SD, shear collapse due to cyclic shear strength degradation; $PGA_u$, peak ground acceleration at RC frame collapse; $PGA_y$, peak ground acceleration at RC column yield; $PGA_j$, peak ground acceleration at beam-column joints failure; $H_{max}$, maximum horizontal base reaction; $d_{max}$, maximum interstorey displacement; $\Delta GAP_c$, maximum relative approaching between the columns and the CLT panel; $\Delta GAP_b$, maximum gap-size variation; symbol Δ, ratio between the value obtained in the retrofit and in the MI configuration.

| Period | Load level | Type | Collapse mechanism | $PGA_y$/g | $PGA_j$/g | $PGA_u$/g | $H_{max}$ (kN) | $d_{max}$ (mm) | $\Delta GAP_c$ (mm) | $\Delta GAP_b$ (mm) | $\Delta PGA_u$ | $\Delta H_{max}$ | $\Delta d_{max}$ |
|---|---|---|---|---|---|---|---|---|---|---|---|---|---|
| '70s | HCL | MI | S | - | - | 0.125 | 155.4 | 7.7 | - | - | - | - | - |
| '70s | HCL | R 10 −20↑ | S | - | 0.25 | 0.25 | 360.1 | 15.0 | 4.8 | 5.8 | 100 % | 132 % | 94 % |
| '70s | HCL | R 10 −55↑ | S | 0.225 | 0.25 | 0.25 | 371.7 | 18.6 | 4.4 | 12.6 | 100 % | 139 % | 140 % |
| '70s | HCL | R 10-NO | S | 0.225 | 0.2 | 0.225 | 347.2 | 21.0 | 4.5 | 3.1 | 80 % | 123 % | 171 % |
| '70s | HCL | R 20 −20 | S | - | 0.175 | 0.175 | 274.2 | 14.3 | 3.7 | 9.1 | 40 % | 76 % | 85 % |
| '70s | HCL | R 20 −55 | S | - | 0.15 | 0.175 | 274.2 | 17.4 | 4.3 | 3.9 | 40 % | 76 % | 125 % |
| '70s | HCL | R 20-NO | S | 0.175 | 0.125 | 0.2 | 265.6 | 23.5 | 3.9 | 3.7 | 60 % | 71 % | 203 % |
| '70s | LCL | MI | S | - | - | 0.3 | 130.4 | 5.4 | - | - | - | - | - |
| '70s | LCL | R 10 −20 | S | 0.6 | 0.65 | 0.8 | 399.2 | 17.8 | 9.6 | 8.8 | 167 % | 206 % | 233 % |
| '70s | LCL | R 10 −55↑ | SD | 0.55 | 0.65 | 0.95 | 443.9 | 25.5 | 4.9 | 14.6 | 217 % | 240 % | 376 % |
| '70s | LCL | R 10-NO | SD | 0.5 | 0.65 | 0.75 | 373.4 | 24.7 | 9.6 | 4.4 | 150 % | 186 % | 362 % |
| '70s | LCL | R 20 −20 | SD | 0.5 | 0.45 | 0.75 | 356.0 | 24.8 | 4.0 | 12.0 | 150 % | 173 % | 363 % |
| '70s | LCL | R 20 −55 | SD | 0.5 | 0.45 | 0.65 | 321.3 | 28.5 | 6.2 | 9.7 | 117 % | 146 % | 432 % |
| '70s | LCL | R 20-NO | SD | 0.35 | 0.4 | 0.5 | 260.8 | 26.3 | 4.6 | 4.8 | 67 % | 100 % | 391 % |
| '60s | HCL | MI | SD | 0.2 | 0.175 | 0.225 | 243.5 | 28.8 | - | - | - | - | - |
| '60s | HCL | R 10 −20↑ | SD | 0.25 | 0.175 | 0.375 | 491.9 | 32.0 | 7.2 | 17.4 | 67 % | 102 % | 11 % |
| '60s | HCL | R 10 −55 | SD | 0.225 | 0.175 | 0.35 | 456.4 | 36.3 | 11.9 | 9.6 | 56 % | 87 % | 26 % |
| '60s | HCL | R 10-NO | SD | 0.2 | 0.175 | 0.3 | 391.2 | 31.1 | 11.6 | 4.3 | 33 % | 61 % | 8 % |
| '60s | HCL | R 20 −20 | SD | 0.2 | 0.15 | 0.275 | 353.4 | 29.4 | 5.0 | 15.1 | 22 % | 45 % | 2 % |
| '60s | HCL | R 20 −55 | SD | 0.2 | 0.125 | 0.275 | 324.8 | 34.5 | 9.8 | 12.2 | 22 % | 33 % | 20 % |
| '60s | HCL | R 20-NO | SD | 0.175 | 0.1 | 0.225 | 277.5 | 34.8 | 8.6 | 6.5 | 0 % | 14 % | 21 % |
| '60s | LCL | MI | SD | 0.45 | 0.45 | 0.55 | 234.7 | 27.6 | - | - | - | | |
| '60s | LCL | R 10 −20↑ | SD | 0.55 | 0.55 | 0.9 | 426.1 | 22.1 | 5.7 | 15.7 | 64 % | 82 % | −20 % |
| '60s | LCL | R 10 −55 | SD | 0.5 | 0.5 | 0.85 | 392.8 | 22.5 | 8.8 | 8.0 | 55 % | 67 % | −18 % |
| '60s | LCL | R 10-NO | SD | 0.4 | 0.5 | 0.75 | 377.9 | 27.3 | 8.8 | 4.0 | 36 % | 61 % | −1 % |
| '60s | LCL | R 20 −20 | SD | 0.45 | 0.35 | 0.7 | 336.6 | 22.6 | 4.2 | 13.3 | 27 % | 43 % | −18 % |
| '60s | LCL | R 20 −55 | SD | 0.45 | 0.4 | 0.6 | 302.8 | 25.8 | 5.5 | 8.0 | 9 % | 29 % | −6 % |
| '60s | LCL | R 20-NO | SD | 0.3 | 0.35 | 0.5 | 259.4 | 29.6 | 6.5 | 5.8 | −9 % | 11 % | 7 % |

frames, the increase in shear action due to higher vertical loads did not entail the shear failure, and therefore a ductile failure due to plastic hinge formation followed by shear strength degradation was observed in both HCL and LCL. Furthermore, the higher vertical load meant larger yielding moments of the columns, and consequently a delayed activation of the shear strength degradation, resulting in increased ultimate drift values (Fig. 15 and Table 10). Lastly, considering the best performing solution among the 60s frames, the increase in vertical loads involved the $\Delta PGA_u$ to move from 64 % (LCL) to 67 % (HCL). On the contrary, considering the best performing 70s frame, the $\Delta PGA_u$ moved from 167 % (LCL) to 100 % (HCL). Therefore, it emerges that in case of sufficient shear reinforcement (i.e., 60s frames), the seismic response is not significantly affected by the column vertical loading. On the other hand, in the case of poor shear strength (i.e., 70s frames), the vertical load on the columns appears to have a significant effect on the overall response.

Based on the analysis results, some general design rules can be defined to further enhance the effectiveness of the retrofit solution. As already mentioned, provided that the beams have sufficient shear overstrength, reducing the spacing between the fasteners along the beams always led to a better seismic response both in terms of $PGA_u$ and $H_{max}$ (Table 10). Regarding the fastener spacing along the columns, although smaller spacings generally resulted in higher column shear demands (Fig. 16), further study on this aspect is recommended. For the 60s frames, the spacing reduction of the column fasteners caused an improvement in the seismic response similar to that observed when reducing the spacing of the beam fasteners. A smaller spacing involved indeed an increase in maximum base shear capacity $H_{max}$, a decrease in drift demand for a given PGA and thus an increase in $PGA_u$ (Fig. 15 and Table 10). Instead, the 70s frames showed different results. Although for reduced spacings of the column fasteners, a decrease in the seismic drift demand is noticeable (Fig. 15), decreases in $H_{max}$ and $PGA_u$ were detected in some cases. In particular, considering the results of 70s-LCL with fastener spaced at 10 cm along the beams (Fig. 15 and Table 10), a 16 % decrease in $PGA_u$ was found when the spacing of the column fasteners was reduced from 55 cm to 20 cm. This result is explained considering Fig. 16 (70s-LCL) and comparing R-10–55 with R-10–20 (shear forces on RC columns). While the R-10–20 curve grows at a constant rate until the shear strength $V_R$ is reached, the R-10–55 curve shows a slope reduction and a subsequent plateau once a certain PGA level is exceeded. This slope reduction is due to the plasticisation of the column ends ($PGA_y$ in Table 10), which limits the increase in shear demand on the columns. Because of such phenomenon, the R-10–55 configuration developed a ductile failure mechanism (due to the column plasticisation), reached a higher PGA level and failed due to shear strength degradation. On the contrary, the R-10–20 configuration showed a brittle collapse mechanism due to shear failure. A less pronounced increase in the column shear demand after a certain PGA threshold was also observed in the 60s frames. Fig. 16 (60s-HCL and 60s-LCL) also shows that smaller spacings for the column fasteners involved higher PGA thresholds at which the curve slope reduction occurs. Because of the larger shear strength of the columns of the 60s frames, the collapse was caused by shear strength degradation even in the cases of smaller spacing (20 cm). In the case of 60s frames, R-10–20 configurations showed the best seismic performance (in terms of $PGA_u$ and $H_{max}$) characterized by shear strength degradation failure for high PGA values (Fig. 16) with relatively small drift demand (Fig. 15).

Regarding the response of the beam-column joints, in 82 % of the frames analysed, the failure of the joints preceded that of the columns or the beams. In all the joint failures detected (identified with $PGA_j$ in Table 10) a tension-governed failure was observed, while compression-

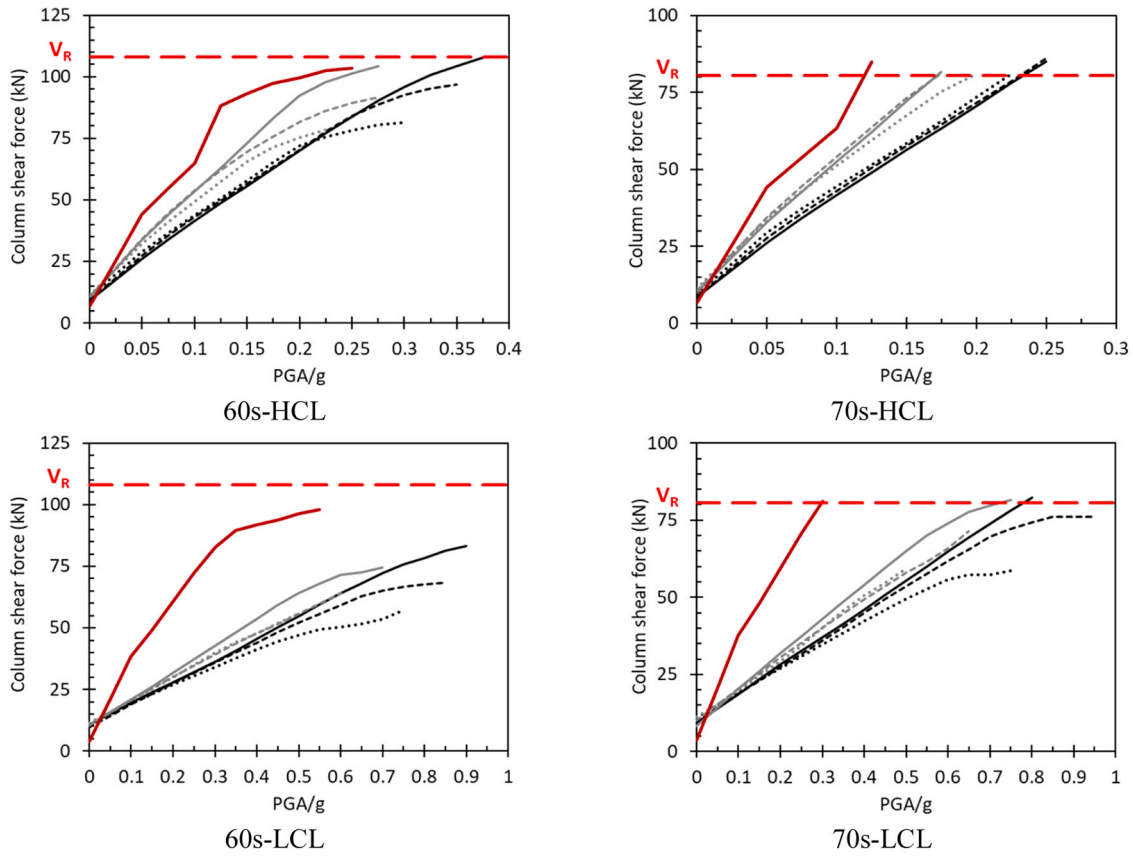


**Fig. 16.** Comparison between as-built and retrofitted configurations – Shear force on the most stressed RC column and related shear strength in the case of no cyclic degradation (VR).

governed failure never occurred. When joint failure was observed for both the masonry-infilled and the retrofitted configurations (i.e., 60s frames), the best performing retrofit configuration showed a PGA at joint collapse ($PGA_j$) equal (60s-HCL) or higher (60s-LCL) than that of the masonry-infilled configuration. This result shows that the retrofit intervention can improve the response of the beam-column joints, confirming the observation by [39]. However, for most of the analysed frames, the retrofit design strategy should include additional strengthening of the joints to guarantee joint overstrength and maximise the benefits of the RC-TP intervention.

Finally, Table 10 reports the maximum variation in the size of the gap between the RC frame and the CLT panel observed in the analyses. In particular, the reported values represent the minimum gap (see Fig. 1) between the panel and the column ($\Delta GAP_c$), and between the panel and the beam ($\Delta GAP_b$) necessary to avoid direct contact during lateral loading. Consistently with the outcome of previous studies [38–42], a gap size equal to 20 mm appears sufficient to avoid contact between the panel and the frame.

## 8. Conclusions

The paper presents the outcome of nonlinear incremental dynamic analyses performed on RC frames retrofitted with a CLT-based strengthening named RC-TP. In the study, the seismic performance of masonry-infilled frames representative of the as-built condition of existing RC frame buildings in Italy was compared to that of frames where the existing infill had been replaced with a structural timber panel. The analyses concerned two sets of frames assumed to have been designed for gravity loads only, considering provisions and typical material properties from two different periods (i.e., the 1960–1970 and 1970–1980 decades). Furthermore, two subsets were created to evaluate the influence of column axial load variation on the seismic response. For each frame, six alternative retrofit configurations, obtained by varying the fastener spacing, were analysed to optimise the effectiveness of the intervention. From the results of the analysis, some general considerations on the efficacy of the retrofit solution and its optimized design were made and are reported in the following.

- The retrofit solution can significantly enhance the seismic performance of infilled RC frames by: a) increasing the PGA at collapse; b) increasing the maximum lateral capacity; c) avoiding brittle collapses due to infill-to-frame local interaction.
- The column load level affects the response of the retrofit intervention mainly in the case of concrete elements with poor shear strength.
- An increased beam shear demand was found associated with the retrofit intervention. However, this increased seismic demand is consistent with the reserve of shear strength present in beams designed solely for gravity loads.
- When different retrofit configurations are compared, increasing the number of fasteners on the beams produces a more considerable enhancement of seismic performance due to a lower column shear demand and an overall increase in base shear capacity.
- The optimal fastener spacing along the columns strongly depends on the column shear strength because increasing the number of fasteners on the columns results in: a) higher base shear capacity and smaller inter-storey drift; b) higher column shear demand.

## CRediT authorship contribution statement

**Andrea Bartolotti:** Conceptualization, Formal analysis, Software, Writing – original draft, Writing – review & editing. **Ivan Giongo:** Conceptualization, Funding acquisition, Supervision, Writing – original

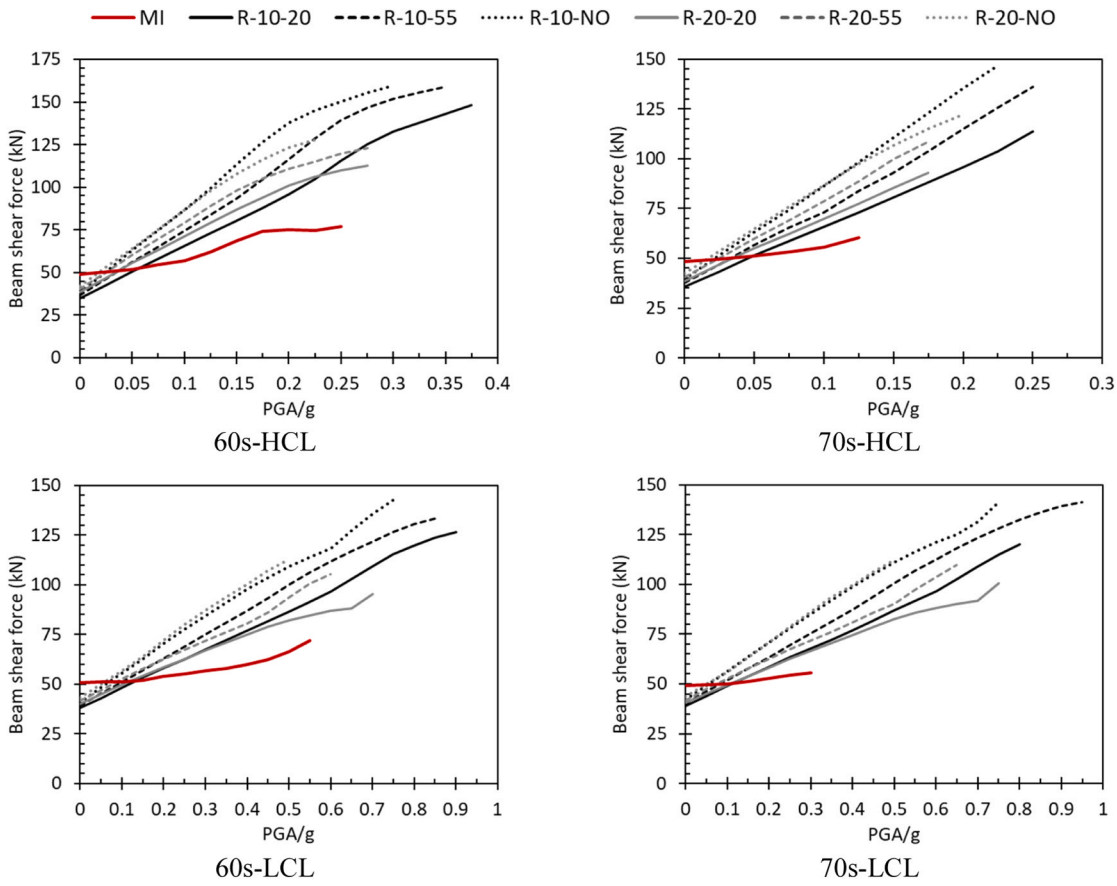


**Fig. 17.** Comparison between as-built and retrofitted configurations – Shear force on the most stressed RC beam.

draft, Writing – review & editing. **Francesco Smiroldo:** Conceptualization, Investigation, Writing – original draft, Writing – review & editing, Supervision.

## Declaration of Competing Interest

The authors declare that they have no known competing financial interests or personal relationships that could have appeared to influence the work reported in this paper.

## Acknowledgements

The authors gratefully thank the 2024–2026 ReLUIS-DPC Project framework (funded by the Italian Emergency Management Agency, DPC) for the financial support given to this study. The authors also acknowledge the Italian Ministry of Universities and Research (MUR), in the framework of the project DICAM-EXC (Departments of Excellence 2023–2027, grant L232/2016).

## References

[1] Kadysiewski S, Mosalam K. Modeling of unreinforced masonry infill walls considering in-plane and out-of-plane interaction, PEER 2008/102. Berkeley: University of California; 2009. p. 144.
[2] Gaetani d'Aragona M, Polese M, Di Ludovico M, Prota A. Seismic vulnerability for RC infilled frames: simplified evaluation for as-built and retrofitted building typologies. Buildings 2018;8(10):137. https://doi.org/10.3390/buildings810013.
[3] Ning N, John Ma Z, Zhang P, Yu D, Wang J. Influence of masonry infills on seismic response of RC frames under low frequency cyclic load. Eng Struct 2019;183: 70–82. https://doi.org/10.1016/j.engstruct.2018.12.083CEN.
[4] Abdelaziz MM, Gomma MS, El-Ghazaly H. Seismic evaluation of reinforced concrete structures infilled with masonry infill walls. Asian J Civ Eng 2019;20: 961–81.
[5] Kallioras S, Pohoryles DA, Bournas D, Molina FJ, Pegon P. Seismic performance of a full-scale five-story masonry-infilled RC building subjected to substructured pseudodynamic tests. Earthq Eng Struct Dyn 2023.
[6] CEN. EN 1998-1. Eurocode 8: design of structures for earthquake resistance. Part 1: general rules, seismic actions and rules for buildings.. 2004.
[7] ACI (American Concrete Institute). ACI 318-19 & ACI 318R-19: building code requirements for structural concrete and commentary. Michigan, USA: American Concrete Institute; 2019.
[8] NTC (2018) D.M. 17/01/2018 - New technical standards for buildings, Official Journal of the Italian Republic, 17th January 2018 (In Italian).
[9] Sezen H, Whittaker AS, Elwood KJ, Mosalam KM. Performance of reinforced concrete buildings during the August 17, Kocaeli, Turkey earthquake, and seismic design and construction practise in Turkey. Eng Struct 2003;25(1):103–14.
[10] Ricci P, De Luca F, Verderame GM. 6th April 2009 L'Aquila earthquake, Italy: reinforced concrete building performance. Bull Earthq Eng 2011;9(1):285–305.
[11] Masi A, Chiauzzi L, Santarsiero G, Manfredi V, Biondi S, Spacone E, Verderame GM. Seismic response of RC buildings during the Mw 6.0 August 24, 2016 Central Italy earthquake: the Amatrice case study. Bull Earthq Eng 2019; 17.10:5631–54.
[12] Demirel IO, Yakut A, Binici B. Seismic performance of mid-rise reinforced concrete buildings in Izmir Bayrakli after the 2020 Samos earthquake. Eng Fail Anal 2022; 137:106277.
[13] Hashemi S, Mosalam K. Seismic evaluation of reinforced concrete buildings including effects of infill masonry walls, 100. Pacific Earthquake Engineering Research Center, PEER; 2007. p. 1026–37.
[14] Pallarés FJ, Davia A, Hassan WM, Pallarés L. Experimental and analytical assessment of the influence of masonry façade infills on seismic behavior of RC frame buildings. Eng Struct 2021;235:112031.
[15] Negro P, Colombo A. Irregularities induced by nonstructural masonry panels in framed buildings. Eng Struct 1997;19(7):576–85.
[16] Verderame GM, De Luca F, Ricci P, Manfredi G. Preliminary analysis of a soft-storey mechanism after the 2009 L'Aquila earthquake. Earthq Eng Struct Dyn 2011;40(8):925–44.
[17] Dolšek M, Fajfar P. Soft storey effects in uniformly infilled reinforced concrete frames. J Earthq Eng 2001;5(01):1–12.
[18] Paulay T, Priestley MN. Seismic Design of Reinforced Concrete and Masonry Buildings, Vol 768. New York: Wiley; 1992.
[19] Crisafulli F. Seismic Behaviour of Reinforced Concrete Structures with Masonry Infills. New Zealand: PhD Thesis, University of Canterbury; 1997.

[20] Basha SH, Kaushik HB. A novel macromodel for prediction of shear failure in columns of masonry infilled RC frames under earthquake loading. Bull Earthq Eng 2019;17:2219–44.
[21] Blasi G, De Luca F, Aiello MA. Brittle failure in RC masonry infilled frames: The role of infill overstrength. Eng Struct 2018;177:506–18.
[22] Cagatay IH, Beklen C, Mosalam KM. Investigation of short column effect of RC buildings: failure and prevention. Comput Concr 2010;7(6):523–32. https://doi.org/10.12989/cac.2010.7.6.523.
[23] Da Porto F, Guidi G, Verlato N, Modena C. Effectiveness of plasters and textile reinforced mortars for strengthening clay masonry infill walls subjected to combined in-plane/out-of-plane actions / Wirksamkeit von Putz und textilbewehrtem Mörtel bei der Verstärkung von Ausfachungswänden aus Ziegelmauerwerk, die kombinierter Scheiben- und Plattenbeanspruchung ausgesetzt sind. Mauerwerk 2015;19(5):334–54. https://doi.org/10.1002/dama.201500673.
[24] Ezzatfar P, Binici B, Kurç Ö, Canbay E, Sucuoğlu H, Özcebe G. Application of mesh reinforced mortar for performance enhancement of hollow clay tile infill walls. Seismic Evaluation and Rehabilitation of Structures. Springer; 2014. p. 171–86.
[25] Pohoryles DA, Bournas DA. Seismic retrofit of infilled RC frames with textile reinforced mortars: State-of-the-art review and analytical modelling. Compos Part B: Eng 2020;183:107702.
[26] Preti M, Bolis V, Stavridis A. Design of masonry infill walls with sliding joints for earthquake structural damage control. In: Proceedings of the 16th International. Brick Block Mason Conf (IBMAC'16) Padova, Italy 2016.
[27] Cao XY, Shen D, Feng DC, Wang CL, Qu Z, Wu G. Seismic retrofitting of existing frame buildings through externally attached sub-structures: State of the art review and future perspectives. J Build Eng 2022;57:104904.
[28] Gkournelos PD, Triantafillou TC, Bournas DA. Seismic upgrading of existing reinforced concrete buildings: a state-of-the-art review. Eng Struct 2021;240:112273.
[29] Pohoryles DA, Bournas DA, Da Porto F, Caprino A, Santarsiero G, Triantafillou T. Integrated seismic and energy retrofitting of existing buildings: A state-of-the-art review. J Build Eng 2022;Vol 61:105274. https://doi.org/10.1016/j.jobe.2022.105274.
[30] Baek E, Pohoryles DA, Kallioras S, Bournas DA, Choi H, Kim T. Innovative seismic and energy retrofitting of wall envelopes using prefabricated textile-reinforced concrete panels with an embedded capillary tube system. Eng Struct 2022;265:114453. https://doi.org/10.1016/j.engstruct.2022.114453.
[31] Iovane G., Sandoli A., Marranzini D., Landolfo R., Prota A., Faggiano B. Timber based systems for the seismic and energetic retrofit of existing structures. Procedia Structural Integrity, Vol 44, pages 1870–1876, https://doi.org/10.1016/j.prostr.2023.01.239.
[32] Sustersic I. and Dujic B. Seismic shaking table testing of a reinforced concrete frame with masonry infill strengthened with cross laminated timber panels. In: World Conference on Timber Engineering. Quebec City, Canada, 10–14 August; 2014.
[33] Margani G, Evola G, Tardo C, Marino EM. Energy, seismic, and architectural renovation of RC framed buildings with prefabricated timber panels. Sustainability 2020;12:4845. https://doi.org/10.3390/su12124845.
[34] Aloisio A, Pellicciari M, Sirotti S, Boggian F, Tomasi R. Optimization of the structural coupling between RC frames, CLT shear walls and asymmectric friction connections. Bull Earth Eng 2022;20:3775–800.
[35] Mehdipour Z, Poletti E, Branco JM, Lourenco P. Numerical analysis of masonry-infilled RC-CLT panel connections. Buildings 2022;12(11). https://doi.org/10.3390/buildings12112009.
[36] Stazi F, Serpilli M, Maracchini G, Pavone A. An experimental and numerical study on CLT panels used as infill shear walls for RC buildings retrofit. Constr Build Mater 2019;211:605–16. https://doi.org/10.1016/j.conbuildmat.2019.03.196.
[37] Suga J., Ono M., Aoki K., Fukuhara T., Kurihara T., Maeda T. Timber Shear Walls for Seismic Retrofit of Reinforced Concrete Buildings. In: World Conference on Timber Engineering. Seoul, Republic of Korea, 20–23 August; 2018.
[38] Smiroldo F, Giongo I, Piazza M. Use of timber panels to reduce the seismic vulnerability of concrete frame structures. Eng Struct 2021;0244:112797.
[39] Smiroldo F., Giongo I., Piazza M. Seismic retrofit of masonry infilled frames by using timber panels. In: Proceedings of the 17th World Conference on Earthquake Engineering (17WCEE). Sendai, Japan. 2020:13–18.
[40] Smiroldo F., Viel D., Giongo I., Piazza M. A numerical study on a timber-based retrofit intervention for masonry infilled concrete frames. In: 8th ECCOMAS Thematic Conference on Computational Methods in Structural Dynamics and Earthquake Engineering. Athens, Greece. 2021.
[41] Smiroldo F, Paviani I, Giongo I, Zanon S, Albatici R, Piazza M. An integrated approach to improve seismic and energetic behaviour of RC framed buildings using timber panels. Sustainability 2021;13(20).
[42] Smiroldo, F.; Kallioras S.; Sommacal, G.; Bournas D.; Piazza M.; and Giongo I.: Full-scale testing of Masonry-Infilled RC Frames retrofitted with Cross-Laminated Timber Panels. Eng. Struct., 294, p. 116789. https://doi.org/10.1016/j.engstruct.2023.116789.
[43] ISTAT. 154° Censimento della Popolazione e delle Abitazioni. 2011. (In Italian).
[44] R.D.L. 16 NOVEMBRE 1939 N°2228–2232 (Suppl. Ord. alla Gazz. Uff. del 18 aprile 1940 n°92) Norme per l'esecuzione delle opere in conglomerato cementizio semplice od armato. (In Italian).
[45] CIRCOLARE 23 MAGGIO 1957 N°1472, Armature delle strutture in cemento armato. (In Italian).
[46] DECRETO MINISTERIALE 30/5/1972, Norme tecniche alle quali devono uniformarsi le costruzioni in conglomerato cementizio, normale e precompresso ed a struttura metallica. (In Italian).
[47] Santarella L. Il cemento armato. Milano: Ulrico Hoepli; 1959 (In Italian).
[48] Colombo G., Cucco L., Rossi C. Manuale dell'ingegnere civile e industrial. Milano: Hoepli; 1968. (In Italian).
[49] Verderame G.M., Ricci P., Esposito M., Sansiviero F.C. Le caratteristiche meccaniche degli acciai impiegati nelle strutture in ca realizzate dal 1950 al 1980. In: XXVI Convegno Nazionale AICAP. Padova, Italy. 2011. (In Italian).
[50] Ghersi A, Lenza P. Edifici esistenti in cemento armato. Valutazione e mitigazione del rischio sismico.. Palermo: Dario Flaccovio Editore; 2020 (In Italian).
[51] Cristofaro M.T., D'Ambrisi A., De Stefano M., Pucinotti R., Taganelli M. Analisi statistica sulla dispersione dei valori della resistenza a compressione del calcestruzzo prelevato da edifici esistenti. In: 14° Congresso AIPnD, Conferenza nazionale sulle prove non distruttive monitoraggio diagnostica. Firenze, Italy. 2011. (In Italian).
[52] "Ministero delle Infrastrutture e dei Trasporti. CNTC19 - Circolare applicativa delle Norme Tecniche delle Costruzioni di cui al D.M. 17/01/2018 (NTC 2018). Italy: Gazzetta Ufficiale N. 42 del 20/ 02/2018 (in Italian); 2019." (In Italian).
[53] Computers and Structures Inc., SAP 2000 Integrated Software for Structural Analysis and Design, Walnut Creek, California, USA.
[54] Mander JB, Priestley MJ, Park R. Theoretical stress-strain model for confined concrete. J Struct Eng 1988;114(8):1804–26.
[55] Liberatore L, Noto F, Mollaioli F, Franchin P. In-plane response of masonry infill walls: comprehensive experimentally-based equivalent strut model for deterministic and probabilistic analysis. Eng Struct 2018;167:533–48. https://doi.org/10.1016/j.engstruct.2018.04.057.
[56] Dowell O, Seible F, Wilson EL. Pivot hysteresis model for reinforced concrete members. Acids Struct J 1998;95:607–17.
[57] Cavaleri L, Di Trapani F. Cyclic response of masonry infilled RC frames: experimental results and simplified modeling. Soil Dyn Earthq Eng 2014;65:224–42. https://doi.org/10.1016/j.soildyn.2014.06.016.
[58] FEMA. Prestandard and commentary for the seismic rehabilitation of buildings. Rep. No. 356. Washington, D.C.: Federal Emergency Management Agency (FEMA); 2000.
[59] Cavaleri L, Di Trapani F. Prediction of the additional shear action on frame members due to infills. Bull Earthq Eng 2015;13(5):1425–54. https://doi.org/10.1007/s10518-014-9668-z.
[60] Rinaldin G, Herve Poh'sie G, Amadio C, Fragiacomo M. Modelling the seismic behaviour of light-frame timber structures. Ingegneria Sismica. Int J Earthq Eng December 01, 2013;4:82–98 (Italy).
[61] Porcu MC, Bosu C, Gavrić I. Non-linear dynamic analysis to assess the seismic performance of cross-laminated timber structures. J Build Eng 2018;19:480–93. https://doi.org/10.1016/j.jobe.2018.06.0087.
[62] Smiroldo F., Sommacal G., Kallioras S., Bournas D., Piazza M., Giongo I. Material characterisation for the numerical modelling of a timber-based seismic retrofit for RC buildings. In: Proceeding of XIX ANIDIS Conference. Torino, Italy. 2022.
[63] Vamvatsikos D, Cornell CA. Incremental dynamic analysis. Earthq Eng Struct Dyn 2002;31(3):491–514. https://doi.org/10.1002/eqe.141.
[64] Ancheta TD, Darragh RB, Stewart JP, et al. NGA-West2 Database. Earthq Spectra 2014;30(3):989–1005. https://doi.org/10.1193/070913EQS197M.
[65] Consiglio dei Ministri. Regio Decreto Legge n. 2229 del 16/11/1939. G.U. n.92 del 18/04/1940. 1939.
[66] Priestley MJ Nigel, Verma Ravindra, Xiao Yan. Seismic shear strength of reinforced concrete columns. J Struct Eng 1994;120(8):2310–29. https://doi.org/10.1061/(ASCE)0733-9445(1994)120:8(2310).
[67] Biskinis DE, Roupakias GK, Fardis MN. Degradation of shear strength of reinforced concrete members with inelastic cyclic displacements. Struct J 2004;101(6):773–83.